Theoretical research aiming at high-efficiency hydrogen production using solar thermochemical energy for the goal of sustainable energy supply

Takaki Nishimura[1], Tatsuya Kodama[2], Genta Sakane[3], & Tomohiko Ishii[1]

[1]Department of Advanced Materials Science, Graduate School of Engineering, Kagawa University, 2217-20 Hayashi-cho, Takamatsu, Kagawa 761-0396, Japan,

[2]Department of Engineering, Niigata University, 8050 Igarashi 2no-cyo, Nishi-ku, Niigata 950-2181, Japan

[3]Department of Chemistry, Faculty of Science, Okayama University of Science, 1-1 Ridaicho, Kita-ku, Okayama 700-0005, Japan

s20d552@stu.kagawa-u.ac.jp.

Ⅰ. Abstract

This study aims to theoretically explain the experimental facts of the thermal redox reaction by means of the first principle calculation called Discrete Variational X α (DV-X α) molecular orbital calculation. It is indicated that the relation between the effects of the transition metal doping into cerium oxide (CeO_2: ceria) and the hydrogen gas production in the thermal redox reaction. The calculation results showed that the bonding between the metal ions and the oxygen ions in the doped ceria is stronger than that shown in the non-doped ceria. In addition, the Mndoped ceria showed the most robust bonding among the transition metal (Mn, Fe, Co, Ni) doped ceria. These results suggested that the magnitude of the crystal structure stabilization affects the redox reaction efficiency in each doped ceria. We summarized that the bonding strength in the doped ceria is one of the critical points considering the redox reaction efficiency.

I-1. Introduction

Novel energy styles and energy productions are so required, hydrogen energy has been much attraction from the viewpoint of the environment. Many utilities of the hydrogen energy have been studied, and industry studies of the hydrogen have also been done [1-4]. In Fig. 1, it is shown that the hydrogen production facility in Jülich, Germany. The "Green hydrogen technologies" project has been demonstrated [5-7], and the hydrogen gas has been sourced continuously from solar heat [8-10]. It has the advantage of storing sustainable "solar energy", which can be irradiated from the sun to the earth in the form of "hydrogen energy". So, it makes good sense to convert intermittently solar energy (clean energy) to hydrogen energy (clean energy). Considering these points, Kodama et al. have studied new energy production of the solar thermochemical production by an oxidation-reduction reaction of the cerium oxide (CeO_2: ceria) [11-12]. In

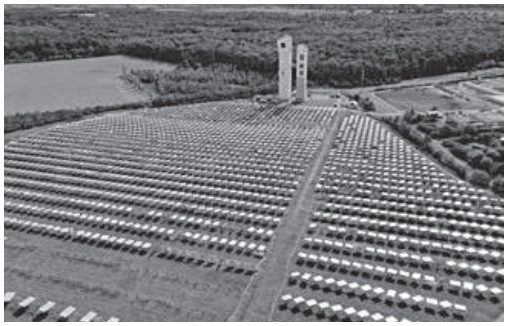

Figure 1. DLR concentrated solar thermal test site at Jülich image@DLR (Ref: SolarPACES)

Fig. 2, the hydrogen gas production facility uses the solar thermochemical process at Miyazaki University in Japan [13]. The flow of the hydrogen production is shown in Fig. 3. Then, the sunlight can be concentrated by many heliostats and converted to thermal energy. The thermal redox reaction can generate a hydrogen gas with control of the reaction temperature. Moreover, the redox reaction is the cycle reaction that consists of twostep reactions, which makes it possible to produce the hydrogen gas efficiently. If the solar energy can be supplied stably, we can get hydrogen energy continuously.

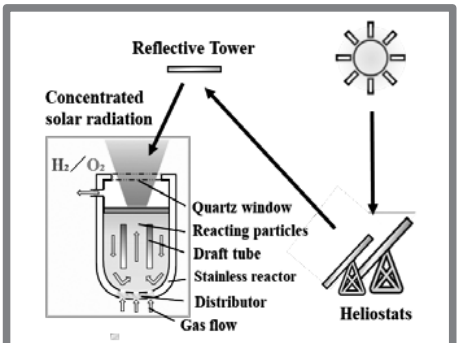

Figure 3. Floor plan of solar reactor concept for a circulating reaction measure.

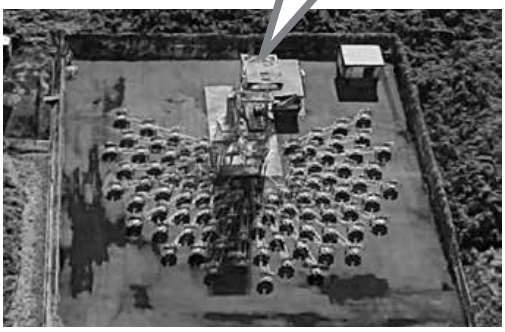
Figure 2. The solar thermochemical production at Miyazaki University. (Ref: Google map.)

The two-step thermal redox reaction is used for the hydrogen gas production; much research has been done up to now [11-14]. The two-step thermal redox reaction has the reduction reaction (1st step: eqn.1) with oxygen desorption at high temperatures (>1,000℃)and the oxidation reaction (2nd step: eqn.2) with oxygen adsorption at low temperatures (< 1,000 ℃). In the thermal oxidation reaction (2nd step), water molecules gas can be decomposed under high-temperature steam, and the hydrogen can be produced efficiently [15-16].

$$\text{1st step: } M_xO_y \rightarrow M_xO_{y-\delta} + \delta/2\ O_2 \text{ (eqn.1)} \cdots \text{Thermal Reduction (TR) reaction}$$
$$\text{2nd step: } M_xO_{y-\delta} + \delta\ H_2O \rightarrow M_xO_y + \delta\ H_2 \text{ (eqn.2)} \cdots \text{Water Decomposition (WD) reaction}$$

In the experimental results, Kodama *et al.* reported that the thermal redox reactivity and cyclicality increase in the case of the Mn or Fe-doped ceria [17-18]. It was suggested that the transition metal doping would cause electronic state change into ceria. Theoretically, it is crucial to clarify the difference in the hydrogen production activity in the thermal redox reaction due to the transition metal doping.

The thermal redox reaction is the oxygen adsorption/desorption reaction. The hydrogen and oxygen gases production is associated with the oxygen absorption reaction (WD reaction) and the oxygen desorption reaction (TR reaction). These reactions indicate the bonding state changes between the metal ions and the oxygen ions in the ceria. The thermal redox reaction can be referred to as the oxygen adsorption/desorption reaction. Therefore, it was considered that the effect of doping transition metals into ceria could be explained theoretically by clarifying the differences in the bonding states between metal ions and oxygen ions. The Discrete Variational X α (DV-X α) molecular orbital calculation method was used for evaluating the bonding strength.

I-2. Calculation method

The DV-X α molecular orbital calculation (DV-X α method) was developed by D. E. Ellis and H.

Adachi [19-22]. The electronic potential of the DV-X α method is proposed as "X α potential" by J. C. Slater. It is one of the advantages that the DV-X α method has numerically evaluated a substance's electronic state. Therefore, the *d* or *f*-orbitals of metal ions can be accurately calculated. This study focuses on the bonding state between metal and oxygen ions. The accurate calculation of the metal's *d* or *f*-orbitals is critical.

The calculation model is the $M@Ce_{12}O_8^{36+}$ cluster model composed of 12 cerium tetravalent ions (Ce^{4+}) and 8 oxygen ions (O^{2-}), in which the central ion is substituted with another metal ions (M^{4+}), M = Ce (non-substitution) and M = Mn, Fe, Co, and Ni (substitution). The reported experimental data determined the cluster models [17-18]. The cluster model ($M@Ce_{12}O_8^{36+}$) has the fluorite type structure (Fm-3m) with the lattice constant of 5.411 Å. It has the substituted central metal ions (M^{4+}), the 8 oxygen ions around the central ion, and additional 12 cerium ions located outside each oxygen ion.

Moreover, the oxygen ion defect models are also prepared. The prepared models are the $M@Ce_{12}O_7^{36+}$ cluster models. The cluster model ($M@Ce_{12}O_7^{36+}$) corresponds with an oxygen ion desorbed from the previous cluster models ($M@Ce_{12}O_8^{36+}$) after taking two electrons into calculations. The lattice constant is assumed to change with the oxygen adsorption/desorption reaction (WD/TR reaction) processes. Therefore, calculations were also performed for the two cluster models ($M@Ce_{12}O_8^{36+}$ and $M@Ce_{12}O_7^{36+}$) with varying the lattice constants around 5.411 Å (5.250 Å to 5.600 Å). On the computational run of the DV-X α method, the atomic positions are not to change comparing between before and after calculating the cluster models. Taking advantage of this calculation condition, we considered it helpful for examining the effect of the oxygen desorption for each metal-doped model.

The calculations are performed self-consistently until the difference in orbital populations between the initial and final states of the iteration is less than 0.0005 electrons. The calculations were also performed considering the Madelung potential in each cluster model.

Ⅱ. Results & Discussion

In this study, to discuss the stabilization of the metal-doped crystal structure, we considered the bonding strength between the doped central metal ion and the surrounding oxygen ions in the cluster models ($M@Ce_{12}O_8^{36+}$ and $M@Ce_{12}O_7^{36+}$). We discussed the stability of the crystal structure in the doped ceria by comparing it with the BOP values, as explained below.

It was evaluated that the magnitude of the bonding strength between the central metal ions and the oxygen ions by means of calculated parameter called the Bond Overlap Population (BOP). The BOP means how much electrons are occupied in bonding orbitals. If the BOP value becomes larger, there is more overlap in the wave functions between the two atoms, which becomes a strong bonding.

Ⅱ-1. The $M@Ce_{12}O_8^{36+}$ cluster models without oxygen defect (before TR reaction / after WD reaction products)

In this part, it is shown the calculation results without the oxygen defect models. The models

correspond to the sample obtained in the experiment, before TR reaction / after WD reaction products. In Table 1, the BOP values are shown in each $M@Ce_{12}O_8^{36+}$ type cluster model, M = Ce (non-substitution) and M = Mn, Fe, Co, and Ni (substitution). The horizontal cells show the type of the doped metal, and the vertical items show the lattice constants (Å). The lattice constant of the doped metal was varied from 5.250 Å to 5.600 Å.

Table 1. The BOP values for the $M@Ce_{12}O_8^{36+}$ cluster models (M = Ce, Mn, Fe, Co, Ni).

Bond Overlap Population Value (BOP) for the $M@Ce_{12}O_8^{36+}$ cluster models												
Lattice Constant (Å)	5.250	5.300	5.350	5.400	5.411	5.420	5.425	5.430	5.435	5.450	5.500	5.600
M = Ce (pure ceria)	0.261	0.409	0.541	0.679	0.681	0.681	0.712	0.722	0.733	0.763	0.857	1.011
M = Mn (Mn-doped)	1.456	1.460	1.459	1.463	1.463	1.463	1.461	1.460	1.459	1.456	1.445	1.413
M = Fe (Fe-doped)	1.400	1.401	1.399	1.401	1.400	1.400	1.398	1.397	1.396	1.393	1.380	1.346
M = Co (Co-doped)	1.317	1.321	1.321	1.325	1.324	1.324	1.322	1.322	1.321	1.318	1.307	1.277
M = Ni (Ni-doped)	1.185	1.190	1.191	1.196	1.196	1.196	1.194	1.194	1.193	1.191	1.182	1.156

In Table 1, the BOP value changes are shown in the doped metal with the lattice constant changes. The lattice constants between 5.400 and 5.420 (Å) resulted in higher BOP values. On the other hand, as the lattice constant increased, the BOP values also increased in the undoped ceria. It is probably that the 4*f* orbitals of the cerium outermost shell orbitals do not overlap well with the 2*p* orbitals of oxygen. Therefore, when the lattice constant was expanded, the interelectron repulsion between the cerium and the oxygen ions decreased, and the BOP values increased.

The BOP values were large in transition metal-doped ceria than that in undoped ceria. Remarkably, the bonding strength was determined by the doped metal species from Table 1. It meant that the transition metals doping into ceria would stabilize the ceria crystal structure (space group: Fm-3m). It was apparent that the bonding between the Mn ion and the oxygen ions becomes stronger than the Fe, Co, and Ni-doped ceria. While such results were obtained, it also suggested that even in those of the Mn-doped ceria, when the metal doping amount was a few moles, the oxygen ions around the Ce ions are easily defected rather than that around the Mn ions. This is because the BOP values are lower in the undoped ceria. The bonding between the central cerium ion and the oxygen ions can easily deviate.

Moreover, Kodama *et al.* reported that the Mn or Fe-doped ceria shows the stoichiometric thermal redox reaction, whereas the Co and Ni-doped ceria shows the nonstoichiometric thermal redox reaction [17]. The BOP values are compared with the experimental results of each metal-doped ceria (doped with M = Mn, Fe, Co, Ni). The calculated BOP values of Mn and Fe-doped ceria had larger than that of Co and Ni-doped ceria. From this fact, it was assumed that the doped ceria crystal does not easily collapse while maintaining the oxygen adsorption/desorption capacity. When the bonds are weak, the doped ceria crystal easily collapses. The BOP values suggested that the contribution of doping to the stabilization of the crystal structure of ceria.

II-2. The $M@Ce_{12}O_7^{36+}$ cluster models with the oxygen defect (after TR reaction / before WD reaction products)

Next, it is shown the calculation results with the oxygen defect models. The models correspond to the sample obtained in the experiment, after TR reaction / before WD reaction products. In Table 2, the BOP values are shown in each $M@Ce_{12}O_7^{36+}$ cluster model. Other calculation conditions are the same in the $M@Ce_{12}O_8^{36+}$ cluster models.

Table 2. The BOP values for the $M@Ce_{12}O_7^{36+}$ cluster models (M = Ce, Mn, Fe, Co, Ni).

Bond Overlap Population Value (BOP) for the $M@Ce_{12}O_7^{36+}$ cluster models												
Lattice Constant (Å)	5.250	5.300	5.350	5.400	5.411	5.420	5.425	5.430	5.435	5.450	5.500	5.600
M = Ce (pure ceria)	0.099	0.228	0.344	0.447	0.457	0.474	0.484	0.493	0.502	0.529	0.612	0.744
M = Mn (Mn-doped)	1.257	1.262	1.261	1.256	1.248	1.247	1.246	1.245	1.244	1.242	1.229	1.193
M = Fe (Fe-doped)	1.179	1.180	1.178	1.171	1.163	1.162	1.161	1.160	1.159	1.155	1.142	1.105
M = Co (Co-doped)	1.098	1.096	1.090	1.080	1.072	1.070	1.069	1.068	1.066	1.063	1.048	1.048
M = Ni (Ni-doped)	0.995	0.994	0.988	0.979	0.973	0.971	0.970	0.968	0.967	0.963	0.949	0.913

From Table 2, the lattice constants between 5.250 and 5.350 (Å) resulted in higher BOP values. As the lattice constant increased, the BOP values increased in undoped ceria. Compared to the $M@Ce_{12}O_8^{36+}$ cluster models, the overall values of the BOP were found to decrease in the case of the $M@Ce_{12}O_7^{36+}$ cluster models. This result indicated that the bonding between the doped ion and the surrounding oxygen ions is weakened due to one oxygen ion defect.

It was also found that similar trends as the calculation results of the $M@Ce_{12}O_8^{36+}$ cluster models. The BOP value changes were also remarked at the difference of the doped metal species. The difference in the BOP values was obtained in that the BOP values were large in the transition metal-doped ceria than that in the undoped ceria. The Mn-doped ceria had a stronger bonding than other ceria. These points were the same pattern for the $M@Ce_{12}O_8^{36+}$cluster models. It indicated that the transition metals doping into ceria could stabilize the crystal structure even with an oxygen ion defect. If the crystal structure is unstable and its fluorite structure easily collapses after the TR reaction, the reaction efficiency would show less reactive because it will have small cyclability in the undoped ceria. On the other hand, if the crystal structure is stable without collapse, the reactivity and the cyclability will be enhanced in the metal-doped ceria.

When the transition metals are doped into ceria, the crystal structure becomes more stable. The redox reaction is more likely to proceed without crystal deformation. However, the oxygen adsorption/desorption reaction is considered less likely to proceed when the crystal system becomes excessively stable as the doping amount increases. In other words, it is considered that oxygen elimination is difficult to progress due to the crystal system being excessively stabilized. This correlated with a decrease in the efficiency of the thermal redox reaction when the metal was doped by 30 mol% in the experiments [17-18].

The calculation results showed that the interatomic bonding in Mn or Fe-doped ceria becomes stronger than that in undoped ceria. It makes the crystal structure stabilization more suitable in the thermal redox reaction. Although it may seem contradictory, metal doping contributes to the

thermal reduction reaction while maintaining its oxygen-deficient capacity.

In the oxygen adsorption/desorption reaction, the crystal structure of oxygen-desorbed ceria should remain intact without interfering with the entry and exit of oxygen ions as much as possible. The metal doping into ceria plays a role in both the oxygen desorption and desorption reactions and the stability of the crystal system.

Ⅲ. Conclusion

We have mentioned the theoretical discussion of the two cluster models $M@Ce_{12}O_8^{36+}$ and $M@Ce_{12}O_7^{36+}$considering the doping effects on the ceria. The BOP values between the doped metal ion and the surrounding oxygen ions can predict the bonding stability. From the theoretical calculation results, the Mn-doped ceria has the high ability to maintain the fluorite-type crystal structure among the transition metal doping (M = Ce, Mn, Fe, Co, and Ni). The stabilization of crystal structure also leads to the improvement of the cyclicity and efficiency of the thermal redox reaction. Moreover, the theoretical calculation results are compared with the demonstration experiments. The following correlations were derived.

(1) The large BOP in the Mn and Fe doped ceria relates to the stoichiometric thermal redox reaction.
(2) The small BOP in the Ni and Cu doped ceria relates to the nonstoichiometric thermal redox reaction.

It can be understood that when the bonding is strong, the doped ceria crystal structure does not readily decay, but when the bonding is weak, the doped ceria crystal structure readily decays. We have shown that the BOP values help evaluate the stabilization of the metal-doped ceria with the process of the oxygen adsorption/desorption reaction.

Acknowledgement

The authors appreciate Prof. H. Adachi (Kyoto Univ.) for permission to use a computational program. This work was supported by Grant-in-Aid for Scientific Research (A) (JSPS KAKENHI) Grant Number 20H00362.

Ⅳ. References

(1) Turner, J., Sverdrup, G., Mann, M.K., Maness, P.-C., Kroposki, B., Ghirardi, M., Evans, R.J. and Blake, D. (2008). Renewable hydrogen production. *International Journal of Energy Research*, **32**(5), 379-407.
(2) Chaubey, R., Sahu, S., James, O. O., & Maity, S. (2013). A review on development of industrial processes and emerging techniques for production of hydrogen from renewable and sustainable sources. *Renewable and Sustainable Energy Reviews*, **23**, 443-662.
(3) Dawood, F., Anda, M., & Shafiullah, G. M. (2020). Hydrogen production for energy: An overview. *International Journal of Hydrogen Energy*, **45**(7) , 3847-3869.
(4) Kodama, T. (2019). Japan Aims at Establishing a Hydrogen-Based Society—Can Solar Thermochemistry Contribute? *Journal of Solar Energy Engineering*, **141**(2).

(5) Ball, M., & Wietschel, M.(2009). The future of hydrogen–opportunities and challenges. *International journal of hydrogen energy*, **36**(2),615-627.
(6) Almaraz, S. D. L., Azzaro-Pantel, C., Montastruc, L., & Domenech, S.(2014). Hydrogen supply chain optimization for deployment scenarios in the Midi-Pyrénées region, France. *International journal of hydrogen energy*, **39**(23), 11831-11845.
(7) Reuß, M., Grube, T., Robinius, M., Preuster, P., Wasserscheid, P., & Stolten, D.(2017). Seasonal storage and alternative carriers: A *flexible hydrogen supply chain model*. *Applied Energy*, **200**, 290-302.
(8) Rose, P. K., & Neumann, F.(2020). Hydrogen refueling station networks for heavy-duty vehicles in future power systems. *Transportation Research Part D: Transport and Environment*, **83**, 102358.
(9) Apostolou, D.(2020). Optimisation of a hydrogen production–storage–re-powering system participating in electricity and transportation markets. *A case study for Denmark*. *Applied Energy*, **265**, 114800.
(10) Kluschke, P., & Neumann, F.(2019). Interaction of a Hydrogen Refueling Station Network for Heavy-Duty Vehicles and the Power System in Germany for 2050. *arXiv preprint arXiv*:**1908**.10119.
(11) Kodama, T., Gokon, N., Cho, H. S., Bellan, S., Matsubara, K., & Inoue, K.(2018, November). Particle fluidized bed receiver/reactor with a beam-down solar concentrating optics: Performance test of two-step water splitting with ceria particles using 30-kWth sun-simulator. *In AIP Conference Proceedings* **2033**(1)130009.
(12) Cho, H. S., Myojin, T., Kawakami, S., Gokon, N., Kodama, T., Kang, Y. H., Lee, S.N., Chai, K.K., Yoon, H.K., & Lee, H. J.(2014). Solar demonstration of thermochemical two-step water splitting cycle using CeO2/MPSZ ceramic foam device by 45kWth KIER solar furnace. *Energy Procedia*, **49**, 1922-1931.
(13) Kodama, T., Cho, H. S., Inoue, K., Saito, T., Watanabe, S., Gokon, N., & Bellan, S.(2019, July). Particles fluidized bed receiver/reactor with a beam-down solar concentrating optics: First performance test on two-step water splitting with ceria using a Miyazaki solar concentrating system. *In AIP Conference Proceedings*, **2126**(1), 180011.
(14) Gao, Y., Mao, Y., Song, Z., Zhao, X., Sun, J., Wang, W., Chen, G., & Chen, S.(2020). Efficient generation of hydrogen by two-step thermochemical cycles: Successive thermal reduction and water splitting reactions using equal-power microwave irradiation and a high entropy material. *Applied Energy*, **279**, 115777.
(15) Le Gal, A., Abanades, S., Bion, N., Le Mercier, T., & Harlé, V. (2013). Reactivity of doped ceria-based mixed oxides for solar thermochemical hydrogen generation via two-step water-splitting cycles. *Energy & fuels*, **27**(10), 6068-6078.
(16) Le Gal, A., & Abanades, S.(2011). Catalytic investigation of ceria-zirconia solid solutions for solar hydrogen production. *International Journal of Hydrogen Energy*, **36**(8), 4739-4748.
(17) Gokon, N., Suda, T., & Kodama, T.(2015). Thermochemical reactivity of 5–15 mol% Fe, Co, Ni, Mn-doped cerium oxides in two-step water-splitting cycle for solar hydrogen production. *Thermochimica Acta*, **617**, 179-190.
(18) Gokon, N., Suda, T., & Kodama, T.(2015). Oxygen and hydrogen productivities and repeatable reactivity of 30-mol%-Fe-, Co-, Ni-, Mn-doped $CeO_{2-\delta}$ for thermochemical two-step water-splitting cycle. *Energy*, **90**, 1280-1289.
(19) Adachi, H., Tsukuda, M., & Satoko, C.(1978). Discrete variational Xα cluster calculations. I. Application to metal clusters. *Journal of the Physical Society of Japan*, **45**(3), 875-883.
(20) Satoko, C., Tsukada, M., & Adachi, H.(1978). Discrete variational Xα cluster calculations. Ⅱ. Application to the surface electronic structure of MgO. Journal of the Physical Society of Japan, 45(4), 1333-1360.
(21) Adachi, H., Shiokawa, S., Tsukada, M., Satoko, C., & Sugano, S.(1979). Discrete variational Xα cluster calculations. Ⅲ. Application to transition metal complexes. *Journal of the Physical Society of Japan*, **47**(5), 1528-1537.
(22) Adachi, H., & Taniguchi, K.(1980). Discrete variational Xα cluster calculations. Ⅳ. Application to X-ray emission study. *Journal of the Physical Society of Japan*, **49**(5), 1944-1953.